Non-dimensional assessments to estimate decompression failure in polymers for hydrogen systems

Maximiliano Melnichuk, Frédéric Thiébaud, Dominique Perreux

Non-dimensional assessments to estimate decompression failure in polymers for hydrogen systems

Maximiliano Melnichuk[a,b], Frédéric Thiébaud[a,*], Dominique Perreux[c,a]

a Univ. Bourgogne Franche-Comté, FEMTO-ST Institute, UMR CNRS 6174, Department of Applied Mechanics, 24 Rue de L'Epitaphe, 25000, Besançon, France
b CONICET: Concejo Nacional de Investigaciones Cientıficas y Tecnicas Av, Bustillo 9500, Centro Atomico Bariloche, Bariloche, CP: 8400, Rio Negro, Argentina
c Mahytec SAS, 6 Rue Léon Bel, 39100, Dole, France

Polymer materials subjected to gases at high-pressure can have issues during decompression. For instance, a sudden decompression can promote the formation of cavities inside the material. This phenomenon is known as cavitation or eXposive Decompression Failure (XDF). There is a body of scientific articles discussing different aspects of cavitation phenomenon, which indicate that the degree of damage is proportional to saturation pressure, depressurisation rate, and material thickness, among other parameters.

In this article we propose a general approach by non-dimensional parameters to estimate the risk of cavitation. Numerical results were validated with bibliographic evidence of cavitation in polymers, for both thermoplastics and elastomers. Present results can be used as guidelines for design of systems involving polymers under high pressure, such as o-rings or liners in type IV hydrogen containers.

* *Corresponding author*.
E-mail address: frederic.thiebaud@univ-fcomte.fr (F. Thiébaud).

Introduction

Polymer materials such as elastomers or semicrystalline thermoplastics are susceptible of being permeated by gaseous species under pressure. When the polymer is saturated, an equilibrium conditions is achieved, with internal and external stresses compensated. Then, a sudden decompression can promote the formation of cavities inside the material, which implies its mechanical failure. This phenomenon is known as cavitation or eXposive Decompression Failure (XDF). It is especially relevant in the field of polymer joints for high-pressure systems, ranging from petrochemical applications with methane or carbon dioxide as permeating species [1–3], to high-pressure hydrogen systems [4,5].

Containers type IV is a widely used technology for high-pressure hydrogen applications. It consist of an internal polymer liner acting as a diffusion barrier, a fibre reinforced composite which stands for pressure values up to 1000 bar [6], and a metallic ending for pipe connections. A major issue of such containers is that detachment and inside collapse of the liner was observed during discharge, especially at high rate decompressions [7]. This phenomenon is referred as buckling. Recent publications suggest that cavities formation in the liner might promote such mechanical instability [8,9]. Fig. 1 shows schemes of three main types of damage phenomena: buckling (structural collapse), blistering (localized default) and cavitation (microscopic failure).

Liner materials are frequently polyamides or high-density polyethylene, which have excellent performance as gas-barriers ($D \approx 1 \times 10^{-9}\ m^2\ s^{-1}$), and mechanical performance much higher than that of elastomers used as o-rings. Materials with higher yield stress would have better resistance to cavities formation [10]. Still, as bibliographic evidence shows the occurrence of cavitation in liner materials [8,9], we think that it becomes relevant the study of this phenomenon for the case of hydrogen containers type IV.

According to A. Pawlak, only from 2000 cavitation phenomenon has been recognized as an important factor that determines the way of plastic deformation of polymers [11,12]. Cavitation can be caused by a sudden decompression so as by deformation under severe strain conditions. Among the works dedicated to the cavitation phenomenon, we can point out certain aspects of general consensus: *i*) cavitation phenomenon is observed during pressure descend or discharge stage, never at pressure increase or charge stage [10]; cavitation is promoted by *ii*) higher charge (or saturation) pressure [3,10], *iii*) higher discharge rate [4], *iv*) higher sample thickness [8]; *v*) cavitation is a diffusion-controlled phenomenon [13], which implies that cavities might appear even after decompression [5,14]; *vi*) the diffusivity to mechanical performance ratio is a relevant parameter [8,10]. Considering this last point, it has to be underlined the role of temperature, as diffusion follows an Arrhenius law with temperature ($D = D_0.\exp(-E_d/R.T)$), and it has a strong influence in mechanical properties of polymers [15,16]. Even more, hydrogen containers type IV should be operational in a temperature range $-40\ °C < T < 85\ °C$ [17].

In addition to this, a temperature change can be expected during charge or discharge due to the Joule-Thomson effect. As the thermal conductivity of liner materials is very low ($\approx 1\ W{\cdot}m^{-1}{\cdot}K^{-1}$ [6]; similar to that of a brick) a temperature gradient can be expected, shifting properties inside the liner material. Considering the influence of hydrostatic pressure, some authors estimate that up to 100 bar pressure the effect in transport properties can be disregarded [18]. This is not the case for hydrogen high-pressure systems, which can easily overpass this pressure threshold. Probably because of safety difficulties related to hydrogen at high-pressure, there is a notable lack of parameters indicating the evolution of transport properties of high-pressure hydrogen in polymers [6].

Characterisation of defaults created by a cavitation phenomenon might be a challenge. In 2016, Gerland et al. [19] obtained images of cavities inside PVDF by electron transmission microscopy, showing the self-called nanobubbles with a particle size of 2–3 nm. They studied the synergetic effect of gas decompression and mechanical traction of samples. These results give a picture of which could be the minimum expected size of permanent defaults created by cavitation. Thus, the techniques capable of measuring the bottom range of cavities are limited to TEM microscopy, and x-ray scattering at small and wide angles (SAXS, WAXS) [15,20,21]. Volume change [22,23], acoustic emission [24], tomography [24] and optical microscopy [8,9] are adequate techniques to characterise the upper range of cavities, which in turn can form macroscopic fractures of the polymer, especially after cycling [9,25]. In the case of optical microscopy, resolution is limited to the visible light wavelength: >0.5 μm. While being limited to relatively large cavities, the use of this technique with polarized light has proved to be useful to determine the cavitation effects [8,9], as the created defaults scatter light, causing a whitening effect which can be easily recognized.

From the theoretical models implemented to understand the nature of cavitation phenomenon [13,26,27], we can see

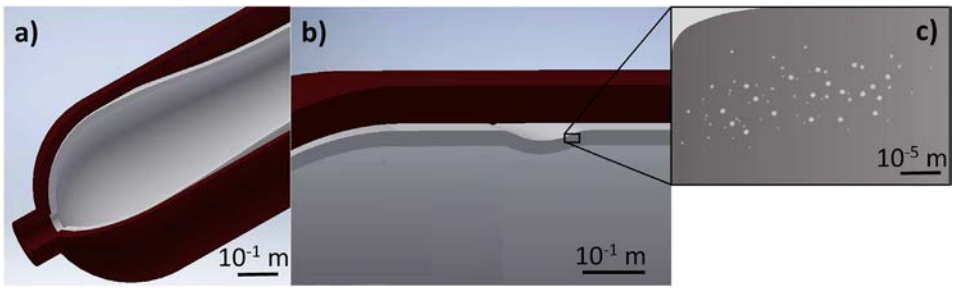

Fig. 1 - Scheme of a hydrogen type IV container under a) buckling, b) blistering, c) cavitation (scale mark is approximate).

that surface tensions effect would destabilize the smaller cavities, causing its collapse, and leaving as permanent deformation cavities having a minimal size [28]. In this sense, from the work of Jaravel et al. [4] we can obtain minimal cavity radius capable of growing to visible size as a function of depressurisation rate.

Considering the importance of cavitation in polymers operating with gases at high-pressure, in this work we propose a general approach by non-dimensional parameters to estimate the risk of cavitation for a generic material, with generic geometry and operational conditions. Validations with bibliographic experimental results confirm that this approach can be useful to predict cavitation, both in thermoplastic and elastomer polymers. As cavitation in polymers is a complex phenomenon, assumptions of the model and its limitations are discussed to better understand the degree of certitude that can be expected from present results.

Numerical model

Numerical model is based in the work made by Yersak et al. published in 2017 [8], which considers the case of a constant rate depressurisation of HDPE samples saturated at 875 bar. The authors were able to match images of optical microscopy showing whitening effect with the pressure inside pre-existent pores, by calculating this pressure by hydrogen concentration calculus and Henry's law. The comparison with the maximal pressure that a core shell would hold determined the cavitation risk.

In our case, we assume a fully saturated sample, immersed in an atmosphere of gas at a certain pressure (P_{ext}), as shown in Fig. 2. We consider the case of a sample with one dimension much smaller than the other two, which would be the case of a disk or a plane sheet of material. On the other hand, fully saturated implies that we assume that the maximum concentration (C_{max}) was achieved for a given saturation pressure (P_{sat}). This concentration is calculated by Henry's law ($C_{max} = P_{sat}/S$). The solubility of the material S is considered to be constant with pressure.

Fig. 3 shows the scheme of the pressure cycle that we consider: we disregard the effect of the pressure increase as we focus our efforts in cavitation phenomenon, which is expected during desorption. We assume that time at P_{sat} was enough to fully saturate the sample, and then we analyse a constant depressurisation rate k, being:

$$k = \frac{(P_{sat} - P_{min})}{(t_{deso} - t_0)} \tag{1}$$

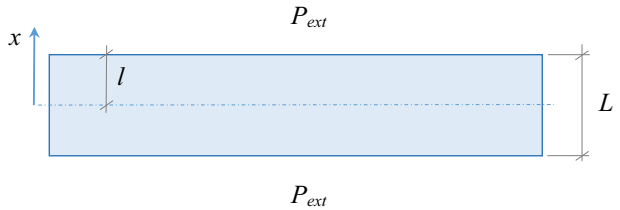

Fig. 2 - Scheme of polymer sample model under gas pressure.

If we assume $t_0 = 0$, then we can use t_{deso} as a single parameter to address characteristic time of the desorption process.

A description of hydrogen concentration evolution is given by equation (2) [8,29]. It considers time and the direction x of diffusion at constant depressurisation rate:

$$\frac{DC}{kl^2} = \frac{Dt}{l^2} + \frac{1}{2}\left(\frac{x^2}{l^2} - 1\right) + \frac{16}{\pi^3}\sum_{n=0}^{\infty}\frac{(-1)^n}{(2n+1)^3} exp\left\{\frac{-D(2n+1)^2\pi^2 t}{4l^2}\right\} cos\frac{(2n+1)\pi x}{2l} \tag{2}$$

where D is the diffusion coefficient, and l is sample half thickness. Here again we considered the diffusion coefficient to be constant with pressure.

The mechanical performance of the polymer was addressed by considering pre-existing defaults of spherical shape, and calculating the maximal pressure that can be hold inside the default before reaching the elastic limit of the material [8,30,31]. A damage criterion was defined by finding the critical load which starts yielding. Fig. 4a illustrates the scheme of a spherical pre-existing default characterised as a thick shell. The pressure at which first yield occurs is defined as follows:

$$P_y = \frac{2}{3}\sigma_y\left(1 - \frac{a^3}{b^3}\right) \tag{3}$$

where P_y is the yield pressure, σ_y is yield stress, a and b are inner radius and outer radius of the shell, respectively. If we consider that the internal radius of the shell is much smaller than its outer radius ($a \ll b$), then the term between parentheses can be disregarded, and we obtain the equation for a spherical pore embedded in a continuum (Fig. 4b):

$$P_y = \frac{2}{3}\sigma_y \tag{4}$$

Damage criteria indicated in equation (4) represents a simplified analysis of the mechanical behaviour of polymers, which present a wide range of strain-stress responses, with viscous, elastic and plastic components. Its mechanical properties are very sensitive to temperature, deformation rate, and environmental conditions. However, as it managed to predict cavitation risk in Ref. [8] under conditions of interest, we adopt it as a first approximation. Moreover, we avoid the discussions related to the size of cavities and its stability in time. Still, it is worth mentioning that some authors

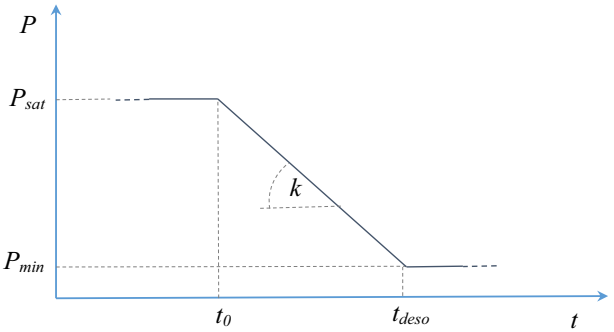

Fig. 3 - Pressure to time cycle considered for calculations.

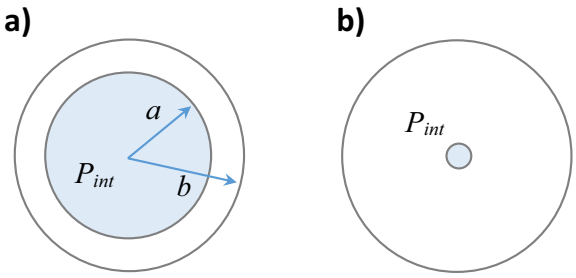

Fig. 4 - Scheme of a spherical shell subjected to hydrostatic internal pressure P_{int}. a) Thick core shell case, b) pore embedded in the continuum case.

considers that as the amorphous part of semicrystalline polymers is where cavitations are created [32], the pre-existence of defaults may not be necessary to start cavitation [24,33]. From this point of view, the spherical default depicted in Fig. 4b would rather be a model to understand the rational base of calculations.

In order to analyse the influence of depressurisation rate, Yersak et al. defined a parameter caller P_{pore}, which accounts the level of unbalance between P_{int} and P_{ext}:

$$P_{pore} = P_{int} - P_{ext} \tag{5}$$

where

$$P_{int} = \frac{C}{S} \tag{6}$$

$$P_{ext} = k.t \tag{7}$$

Fig. 5 shows a scheme with a pore in the central region of a polymer. Part a) of figure represents the moment before depressurisation starts ($k = 0$; $t = t_0$). At this moment, pressure through the entire sample is in equilibrium at P_{sat}. Then depressurisation starts (Fig. 5b), and we consider that P_{ext} descends linearly with time, while P_{int} has a non-linear evolution as in depends on concentration calculated by equation (2). The bigger the depressurisation rate, the bigger the difference between P_{ext} and P_{int}. We also observe in equation (2) that the half thickness l of the sample has a major effect in the gas diffusion phenomenon.

Once we were able to obtain the same results as indicated in Figure 9 of the article of Yersak et al. [8], we moved forward to the non-dimensional approach. Since there is a consensus on many aspects of the cavitation phenomenon, we think that a generalization should be possible. We pursued this generalization by defining the following parameters:

$$T_{deso} = \frac{Dt_{deso}}{l^2} \tag{8}$$

$$M_y = \frac{(P_{sat} - P_{min})}{P_y} \tag{9}$$

$$NDCav = \frac{P_{pore}}{P_y} \tag{10}$$

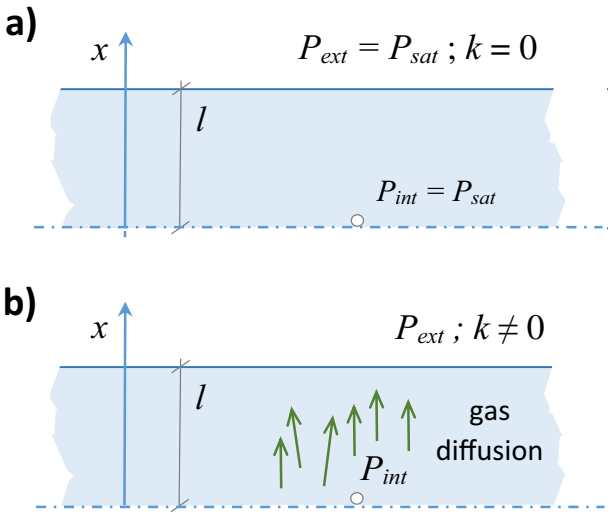

Fig. 5 - Scheme of P_{int} and P_{ext} a) before and b) during depressurisation.

The parameter of equation (8) follows the model of dimensionless parameter used in diffusion problems (see eq (4.21) in Ref. [29]). In this case we consider $t_0 = 0$ and we focus our analysis at $t = t_{deso}$, since during preliminary simulations we observed that the maximum P_{pore} was obtained in times ranging t_{deso}, i.e.: when the difference between P_{int} and P_{ext} would be the highest. It is necessary to mention though that this may not be the case when cavities appearance is observed only after depressurisation, for example for systems depressurizing in a few seconds. Still, given that hydrogen container depressurisation rate is limited to relatively low depressurisation rates (<0.7 MPa min^{-1} [34]), we consider that t_{deso} is a good choice as a characteristic time for our model.

From equation (9) we can notice that the upper part of the fraction considers the total pressure evolution from P_{sat} to P_{min}. The ratio between this pressure value and yield pressure is proportional to the mechanical work considering yield limit (M_y).

Finally, in equation (10) we present in non-dimensional form the yield criterion, by the self-called Non-Dimensional Cavitation (*NDCav*) parameter. When $NDCav > 1$, pore pressure is bigger than yield pressure, thus cavitation can be expected.

From these set of equations we can remark that geometrical parameter (l), and operational parameters (P_{sat}, P_{min} and t_{deso}) are easy to determine and rather stable, thus no relevant as source of incertitude. Contrary, σ_y and D are materials properties very sensible to temperature, and probable to pressure, as discussed in previous section.

Results and validations

Fig. 6 shows the numerical results of T_{deso} vs. M_y, for different *NDCav* curves. The graph indicates the zone where cavitation is unlikely (*NDCav* < 1), and on the other corner the zone where cavitation is highly probable. A transition zone is shaded in between.

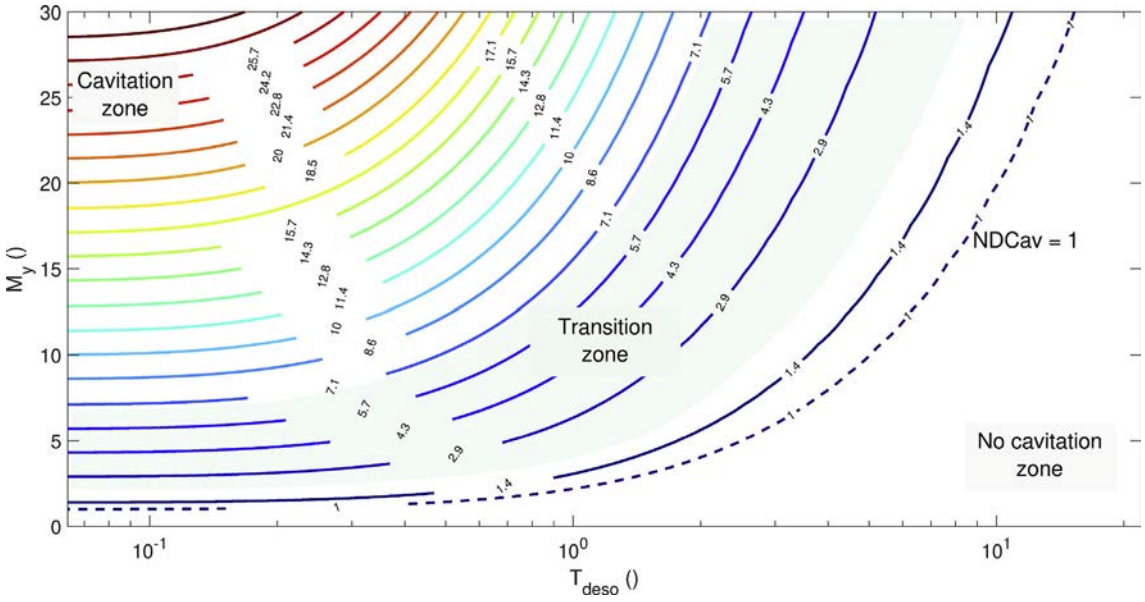

Fig. 6 - Non-dimensional results for cavitation estimation.

Table 1 shows bibliography results for different polymer types, and the respective *NDCav* parameter for comparison. In the "Parameters for calculation" section, we depict the operational and geometric parameters of interest, so as the materials properties in the range of temperature of the experiments. Then non-dimensional parameters T_{deso} and M_y are calculated to obtain *NDCav*. The comparison with bibliography showing images of cavitation failure in the last column is in accordance for both thermoplastics and elastomer polymers. Higher *NDCav* values in Refs. [8,10] correspond with images showing higher density of defaults. In general, values of *NDCav* > 7 correspond with conditions that cause cavitation.

Values of *NDCav* < 2 correspond with experimental results showing no cavitation. At this point we notice a mismatch of our model, as cavitation was expected for *NDCav* < 1. This can be explained by the adopted failure criterion leading to an overestimation of cavitation risk, or by limitations in the characterisation techniques not showing submicronic cavities. The latter is consistent with PA results in Table 1 from

Table 1 - Validation of non-dimensional estimations by comparison with experimental data form bibliography.

Parameters for calculations									Non-dimensional results			Comparison	
Polymer group	Polymer type	*Psat* (MPa)	*Pmin* (MPa)	*tdeso* (min)	*L* (mm)	*σy* (MPa)	*D* (m^2/s)	*T* (°C)	*My* ()	*Tdeso* ()	*NDCav* ()	cavitation	Ref
Thermoplastic	HDPE	87.5	2	60	3.0	7.2[1]	4.00E−10[2]	50	17.8	0.2	16.3	Yes	[8]
		87.5	2	180	3.0	7.2	4.00E−10	50	17.8	0.5	12.2	Yes	[8]
		87.5	2	300	3.0	7.2	4.00E−10	50	17.8	0.8	9.4	Yes	[8]
		87.5	2	780	3.0	7.2	4.00E−10	50	17.8	2.1	4.1	No	[8]
	HDPE	15	0	0.5	2.0	18[3]	2.00E−09[4]	20	1.3	0.02	1.7	No	[8,16]
	HDPE	64.8	0	12	5.4	18[3]	2.00E−09[4]	16	5.4	0.05	5.4	Yes	[8,9]
	PA	64.8	0	12	4.2	45[5]	3.00E−10[6]	16	2.2	0.01	2.6	Yes	[8,9]
Elastomer	EPDM	10	0.1	300	12.5	1.0[7]	3.02E−10[8]	25	14.9	0.03	15	Yes	[2,10]
		5	0.1	300	12.5	1.0	3.02E−10	25	7.4	0.03	7.3	Yes	[2,10]
		2	0.1	300	12.5	1.0	3.02E−10	25	2.9	0.03	2.6	No	[2,10]
		1	0.1	300	12.5	1.0	3.02E−10	25	1.4	0.03	1.7	No	[2,10]
		0.7	0.1	300	12.5	1.0	3.02E−10	25	0.9	0.03	0.8	No	[2,10]

[1] According to Ref. [8] for HDPE at T = 50°C, average value.
[2] According to Ref. [8] for HDPE at T = 50°C.
[3] According to Ref. [8] for HDPE at T = 25°C, average value.
[4] According to Ref. [8] for HDPE at T = 25°C.
[5] According to Ref. [8] for PA at T = 25°C, average value.
[6] According to Ref. [8] for PA at T = 25°C.
[7] According to Ref. [10] for EPDM(NFT) at T = 30°C.
[8] According to Ref. [2] for EPDM at T = 30°C.

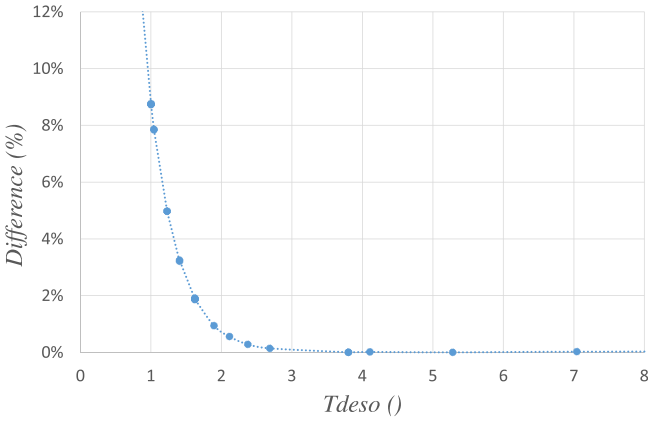

Fig. 7 - Difference between NDCav' values calculated by equation (11) and NDCav values depicted in Fig. 6.

the work of Baldwin [9], showing cavitation evidence after 4 cycles saturation-discharge. The other cited works in the table shows results after only 1 cycle, thus it is possible that for a higher number of cycles, cavitation phenomenon becomes more evident as defaults growth and connect [9].

Intermediate values of *NDCav* between 2 and 7 correspond with bibliographic evidence showing mostly low to moderate damage caused by cavitation. As we can see in Fig. 6, we define this zone as an intermediate zone, given that from the cited works we obtained both cavitation and no-cavitation conditions within this range.

Discussion

As already mentioned, materials properties σ_y and D will play a role in result's sensitivity. We observe a certain dependence of sensitivity on the relative position of Fig. 6. For instance, at low T_{deso} and M_y (lower left zone in the figure), diffusion coefficient variation will not have a major effect in the value of *NDCav*. On the contrary, as *NDCav* curves tend to a vertical position (upper right zone in the figure), yield stress sensibility is lower, thus its variation is not as detrimental. Therefore, the degree of certitude of present results will depend mostly on the accuracy of σ_y and D parameters, especially in the intermediate values zone ($2 < NDCav < 7$). For cases where the model predicts extreme conditions ($2 \gg NDCav$ or $7 \ll NDCav$), results have a higher degree of certitude.

We also made an extension of Fig. 6 to extreme values (not shown), which indicates that for $T_{deso} > 100$ there is no M_y value leading to cavitation. This means, for example, that for desorption times too long, no damage will be caused by the dissolved gas because diffusion will be sufficient to keep P_{pore} values below the failure criterion. On the other hand, values of $M_y < 1$ implies no cavitation for any T_{deso} value. This can be understood as a pressure condition ($P_{sat} - P_{\min}$) mild in comparison to mechanical performance (P_y), thus no damage can be expected.

Finally, as T_{deso} tends to zero (for example, for very thick samples), *NDCav* tend to equal M_y, meaning that the effect of diffusion is irrelevant in comparison with the ratio between pressure condition and mechanical performance. On the other hand, we observe that as T_{deso} increases, *NDCav* becomes a linear function of T_{deso} and M_y according to the following equation:

$$NDCav' = \frac{M_y}{2T_{deso}} \tag{11}$$

Then, Fig. 7 shows the difference between values calculated by equation (11) and the original results calculated to produce Fig. 6 ($Difference = 100\frac{(NDCav - NDCav')}{NDCav'}$). We can see that the difference is smaller than 9% form $T_{deso} > 1$. From $T_{deso} > 2$, this difference becomes <1%. Considering the definition of T_{deso}, this implies that equation (11) is valid within 1% when $\frac{2l^2}{t_{deso}} < D$.

Furthermore, considering equations (4) and (8), and assuming $t_0 = 0$, we can rewrite equation (11) to make a direct calculation of *NDCav*'.

$$NDCav' = \frac{3}{4}\frac{kl^2}{\sigma_y D} \tag{12}$$

Here again, all the discussion related to the *NDCav*' values which implies a risk of cavitation is similar to that of *NDCav*. By the use of equations (11) or (12) when $T_{deso} > 2$, and given that $NDCav \cong M_y$ when $T_{deso} \approx 0$, we end up with a direct method with two equations to calculate *NDCav*, valid in a wide range of conditions. For instance, from the 12 *NDCav* values shown in Table 1, 11 can be calculated by these means.

Conclusions

In the present article, we propose a general method to estimate cavitation risk for polymer materials, with special attention to the case of the liner of hydrogen containers type IV. While damage criteria has strong simplifications considering the actual strain-stress behaviour of polymers, we observe that accordance between our assessments and experimental results found in bibliography is good enough to validate the proposed methodology.

From the analysis of thermoplastics liners in hydrogen containers type IV, we consider that cavitation has to be considered as a relevant factor in the buckling phenomenon. Therefore, present results can be used as a guideline for thermoplastics used as gas barrier.

Our model is consistent with the notion that mechanical performance and diffusivity are relevant properties to the cavitation phenomenon [8,10]. We can add to this discussion that a higher diffusion coefficient would diminish cavitation risk. This implies that a possible strategy to decrease cavitation risk is the use of materials with lower performance as gas barriers, as pressure within pores will decrease faster. In this case, maximum allowed permeation will have to be considered for practical applications.

As future activities, we envisage a further study of the filling rate in unsaturated polymers, as preliminary evaluations suggest that it may play a relevant role in cavitation phenomenon. Even more, we can evaluate other failure criterion models to further understand results when $NDCav \approx 1$.

Acknowledgments

The authors want to thank support from colleagues of University of Franche-Comté/DMA and to the Mahytec team. This work has been supported by the EIPHI Graduate school (contract "ANR-17-EURE-0002"). Financial support has been provided by BPI and Fonds Eruopéen de Développement Régional (FEDER) from Region Bourgogne Franche-Comté, France (Vhyctor project).

REFERENCES

[1] Rueda F, Torres JP, Machado M, Frontini PM, Otegui JL. External pressure induced buckling collapse of high-density polyethylene (HDPE) liners: FEM modelling and predictions. Thin-Walled Struct 2015;96:56–63.
[2] Koga A, Uchida K, Yamabe J. Evaluation on high-pressure hydrogen decompression failure of rubber O-ring using design of experiments. Int. J. Automotive Eng. 2011;2:123–9.
[3] Stewart CW. Nucleation and growth of bubbles in elastomers. J Polym Sci 1970;8(Part -2):937–55.
[4] Yamabe J, Nishimura S. Influence of carbon black on decompression failure and hydrogen permeation properties of filled ethylene-propylene-diene-methylene rubbers exposed to high-pressure hydrogen gas. J. Appl. Polym. Sci. 2011;122:3172–87.
[5] Jaravel J, Castagne S, Grandidier J-C. On key parameters influencing cavitation damage upon fast decompression in a hydrogen saturated elastomer. Benoît G. Polym. Testing 2011;30:811–8.
[6] Barth RR. Polymers for hydrogen infrastructure and vehicle fuel systems: applications, properties, and gap analysis. USA: Sandia National Laboratories; 2013. p. 7–22. Sandia Laboratories report: SAND2013-8904.
[7] Pepin J, Lainé E, Grandidier J-C, Benoit G, Meiller D, Weber M, Langlois C. Replication of liner collapse phenomenon observed in hyperbaric type IV hydrogen storage vessel by explosive decompression experiments. Int J Hydrogen Energy 2018;43:4671–80.
[8] Yersak TA, Baker DR, Yanagisawa Y, Slavik S, Immel R, Mack-Gardner A, Herrmann M, Cai M. Predictive model for depressurization-induced blistering of type IV tank liners for hydrogen storage. Int J Hydrogen Energy 2017;42:28910–7.
[9] Baldwin Don. Development of high pressure hydrogen storage tank for storage and gaseous truck delivery. Hexagon Lincoln: Final report; 2017.
[10] Yamabe J, Koga A, Nishimura S. Failure behavior of rubber O-ring under cyclic exposure to high-pressure hydrogen gas. Eng Fail Anal 2013;35:193–205.
[11] Pawlak A. Cavitation during tensile deformation of high-density polyethylene. Polymer 2007;48:1397–409.
[12] Pawlak A, Galeski A. Cavitation during tensile drawing of annealed high-density polyethylene. Polymer 2010;51:5771–9.
[13] Gent AN, Tompkins DA. Nucleation and growth of gas bubbles in elastomers. J Appl Phys 1969;40:2520–5.
[14] Jaravel J, Castagnet S, Grandidier J-C, Gueguen M. Experimental real-time tracking and diffusion/mechanics numerical simulation of cavitation in gas-saturated elastomers. Int J Solids Struct 2013;50:1314–24.
[15] Piorkowska E, Galeski A. Crystallization of isotactic polypropylene and high-density polyethylene under negative pressure resulting from uncompensated volume change. J Polym Sci Part B 1993;31(10):1285–91.
[16] Melnichuk M, Thiébaud F, Chapelle D, Maynadier A. Etude des propriétés mécaniques des matériaux de réservoirs composites destinés au stockage d'hydrogène. JNC 21-Bordeaux; 2019. p. 6–9.
[17] Barthelemy H, Weber M, Barbier F. Hydrogen storage: recent improvements and industrial perspective. Int J Hydrogen Energy 2017;42:7254–62.
[18] Ho E, Edmond K, Peacock D. Effect of temperature and pressure on permeation, ageing and emissions of elastomers. Seal Technol 2002:5–10.
[19] Gerland M, Boyer S, Castagnet S. Early stages of cavitation in a stretched and decompressed poly(vinylidene fluoride) exposed to diffusive hydrogen, observed by Transmission Electronic Microscopy at the nanoscale. Int J Hydrogen Energy 2016;41:1766–74.
[20] Pawlak A, Krajenta J, Galeski A. Cavitation phenomenon and mechanical properties of partially disentangled polypropylene. Polymer 2018;151:15–26.
[21] Galeski A. Strength and toughness of crystalline polymer systems. Prog Polym Sci 2003;28:1643–99.
[22] Castagnet S, Ono H, Benoit G, Fujiwara H, Nishimura S. Swelling measurement during sorption and decompression in a NBR exposed to high-pressure hydrogen. Int J Hydrogen Energy 2017;42:19359–66.
[23] Miyamoto Y, Nakafuku C, Takemura T. Crystallization of poly(chlorotrifluoroethylene). Polym J 1972;3:122–8.
[24] Kane-Diallo O. Analyse morphologique des champs de cavités dans un élastomère sous décompression d'hydrogène: influence des conditions de décompression et effets d'interaction. Thesis work. Poitiers University; 2016.
[25] Nishimura S. Fracture behavior of ethylene propylene rubber for hydrogen gas sealing under high-pressure hydrogen. Nippon Gomu Kykoishi 2013;12:360–6.
[26] Diani J. Irreversible growth of a spherical cavity in rubberlike material: a fracture mechanics description. Int J Fract 2001;112:151–61.
[27] Gent A, Wang C. Fracture mechanics and cavitation in rubber-like solids. J Material Sci 1991;26:3392–5.
[28] Brennen C. Cavitation and bubble dynamics. Oxford: Oxford University Press; 1995. p. 8.
[29] Crank J. The mathematics of diffusion. 2nd ed. Clarendon Press; 1975. p. 49–56.
[30] Mase G. Schaum's outline of theory and problems of continuum mechanics. McGraw-Hill; 1970.
[31] Prachumchon S. A study of HDPE in high pressure of hydrogen gas – measurements of permeation parameters and failure criteria. Thesis work. University of Nebraska; 2012.
[32] Klopffer M, Berne P, Espuche E. Development of innovating materials for distributing mixtures of hydrogen and natural gas. Study of the barrier properties and durability of polymer pipes. Oil Gas Sci Technol 2015;70:305–15.
[33] Stevenson A, Morgan G. Fracture of elastomers for gas decompression. Rubber Chem Technol 1995;68:197–211.
[34] Pepin J, Lainé E, Grandidier J-C, Castagnet S, Blanc-vannet P, Papin P, Weber M. Determination of key parameters responsible for polymeric liner collapse in hyperbaric type IV hydrogen storage vessels. Int J Hydrogen Energy 2018;43:16386–99.